Available online at www.sciencedirect.com
ScienceDirect
Journal of Photochemistry and Photobiology A: Chemistry 185 (2007) 283–288
Journal of Photochemistry and Photobiology A:Chemistry
www.elsevier.com/locate/jphotochem

A comparative theoretical investigation of ruthenium dyes in dye-sensitized solar cells

Xiao Zhang, Jing-Jun Zhang, Yong-Yao Xia *

Chemistry Department, Shanghai Key Laboratory of Molecular Catalysis and Innovative Materials, Fudan University, Shanghai 200433, China

Received 10 January 2006; received in revised form 26 April 2006; accepted 26 June 2006
Available online 9 August 2006

Abstract

Density functional theory (DFT) and time-dependent DFT method have been employed to analyze the tetradeprotonated complexes of polypyridyl ruthenium dyes *cis*-Ru(4,4′-COOH-2,2′-bpy)$_2$(L)$_2$ (L = NCS, CN and dcbpy; dcbpy = 2,2′-bipyridine-4,4′-carboxylate). The absorption spectra of these complexes in ethanol solution can be well reproduced with theoretical method. The nature of their absorption bands are assigned unambiguously. According to the computational results, energy levels of the singlet and triplet excited states of *cis*-Ru(4,4′-COO$^-$-2,2′-bpy)$_2$(NCS)$_2$ are advantage for the charge injection. Its intense and broad absorption bands as well as favorable excited-state energy levels are key causes for its outstanding efficiency.

Keywords: Dye-sensitized solar cell; Polypyridyl ruthenium dyes; Time-dependent density functional theory

1. Introduction

Dye-sensitized solar cells based on nanocrystalline TiO_2 films are intensively investigated for their low cost and high efficiency [1,2]. The dye acting as photosensitizer is one of the key components for the high efficiency of the cells. Different kinds of dyes, such as organic dyes [3,4] and metal-based dyes [5,6] have been applied in dye-sensitized solar cells. Among these dyes polypyridyl complexes of ruthenium *cis*-Ru(4,4′-COOH-2,2′-bpy)$_2$L$_2$ seem to be the most promising, where L presents a halide, water, cyanide or thiocyanate substituent, etc. [7]. The photosensitizer *cis*-Ru(4,4′-COOH-2,2′-bpy)$_2$(NCS)$_2$, known as N3 dye, shows the most outstanding performance. A new record conversion efficiency of 11.04% was achieved recently by applying guanidinium thiocyanate in the electrolyte [8].

Several factors related to the dyes determine the efficiency of solar cells, such as light harvesting efficiency, quantum yield of charge injection and interfacial charge recombination rate, etc. Numerous experimental researches on ruthenium dyes have been conducted widely; however, theoretical investigations on them remain limited for their comparatively large molecular size. Semi-empirical approaches [9] and density functional theory (DFT) calculations [10] have been applied to ruthenium dyes. Time-dependent density functional theory (TD-DFT) has also been employed for the spectroscopic property analysis of N3 [11], and only very recently its UV–visible spectrum simulation in solvents appeared in the literature [12–15]. Comparative theoretical investigation of ruthenium dyes *cis*-Ru(4,4′-COOH-2,2′-bpy)$_2$L$_2$ (L = NCS, CN, dcbpy; dcbpy = 2,2′-bipyridine-4,4′-carboxylate) with solvation effect still lacks. In this article, we investigated the tetradeprotonated species of [Ru(4,4′-COOH-2,2′-bpy)$_2$(NCS)$_2$], complex **1** [Ru(4,4′-COOH-2,2′-bpy)$_2$(CN)$_2$] (Ru 505) and complex **2** [Ru(4,4′-COOH-2,2′-bpy)$_2$(dcbpy)] (Ru 470, shown in Fig. 1) from the theoretical point of view. The UV–visible absorption spectra in ethanol and some other properties related to the electrochemical process such as their electronic structures and the energy levels of singlet and triplet excited state of dyes are examined in our article in order to elucidate the origin for the outstanding performance of N3.

2. Computational methods

The geometries of $N3^{4-}$ and complexes **1**, **2** have been fully optimized without any symmetry constraints at the B3LYP level of theory with the lanl2dz basis set. TD-B3LYP calcula-

* Corresponding author. Tel.: +86 21 55664177; fax: +86 21 55664177.
E-mail address: yyxia@fudan.edu.cn (Y.-Y. Xia).

1010-6030/$ – see front matter © 2006 Elsevier B.V. All rights reserved.
doi:10.1016/j.jphotochem.2006.06.022

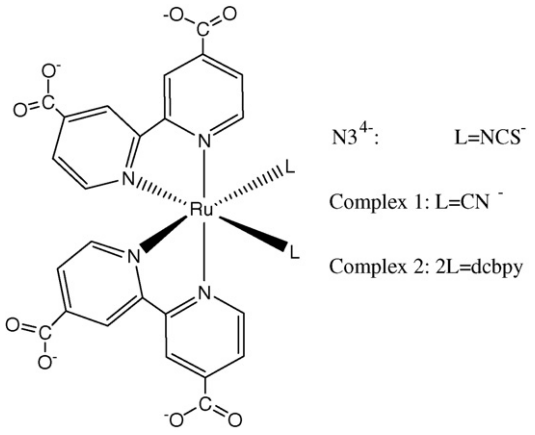

Fig. 1. Molecular structures of the three polypyridyl complexes.

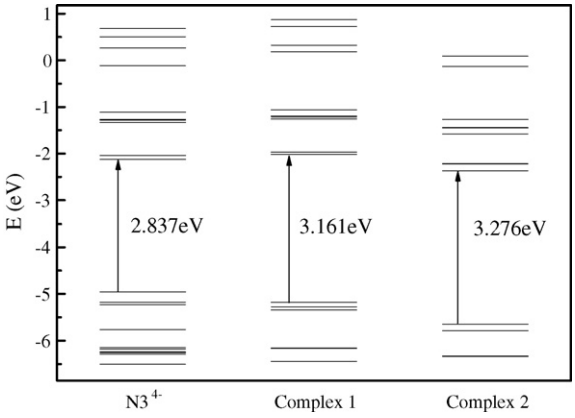

Fig. 2. Energy levels of molecular orbitals of the three complexes.

tion containing solvation effect of ethanol is performed on the geometries optimized in the gas phase. The conductor polarizable continuum model (CPCM) [16,17] is conducted employing parameters and iterative computation methods as suggested by Klamt et al. to contain the Solvation effect. In order to simulate the UV–visible spectra, the 70 lowest spin-allowed singlet transitions are investigated. Transition energetics and oscillator strengths are interpolated by a Gaussian convolution with the full width at half-maximum of 0.4 eV. The energy levels of singlet excited state are calculated consulting the ground-state redox potential and singlet absorption peaks. The energy levels of the first triplet state T_1 state are also estimated with the TD-B3LYP calculation. The Gaussian 03 package of programs was employed throughout this paper [18].

3. Results and discussion

3.1. Geometries

N3^{4-} and its two analogs were studied in this context. As is shown in Fig. 1, they differ in two of their ligands. Some of their optimized geometrical parameters as well as the experimental data [19] are filled in Table 1. The optimized bond lengths of N3^{4-} are longer than those obtained in the X-ray diffraction experiment due to the effect of deprotonation. As cyanide is more liable to share its σ electron towards the empty d orbital of the central metal atom than isothiocyanate, the bonding between cyanide and Ru is stronger. The optimized results show that the distance between Ru and ligand L is shorter for cyanide than isothiocyanate, which is consistent with the foregoing speculation. The distances between Ru and ligand in complex **2** are equal for the equivalency of its three ligands.

Table 1
Part of the optimized geometrical parameters of N3^{4-}, complexes **1** and **2** (in Å)

	N3^{4-}	N3[a] [19]	**1**	**2**
R_{Ru-L}[b]	2.101	2.046–2.048	2.052	2.100
$R_{Ru-bpy(cis)}$[c]	2.077	2.036–2.058	2.142	2.100
$R_{Ru-bpy(trans)}$[d]	2.091	2.013–2.030	2.098	2.100

[a] X-ray experimental results of N3.
[b] R_{Ru-L} represents the distance between Ru and ligand L.
[c] $R_{Ru-bpy(cis)}$ represents the distance between Ru and N atom in bipyridine *cis* to ligand L.
[d] $R_{Ru-bpy(trans)}$ represents the distance between Ru and N atom in bipyridine *trans* to ligand L.

As a whole, there is minor difference between geometrical parameters of the three complexes. Replacement of ligand L has little effect on the molecular structures for this series of complexes, so the notable difference in photoelectric properties of these complexes may root in the effect of ligands on the electronic structures.

3.2. Electronic structures and UV–visible spectra in ethanol

The energy levels of molecular orbitals of these three complexes are summarized in Fig. 2. On going from N3^{4-}, complex **1** to complex **2**, the energy levels of their HOMO orbitals become negative, which is consistent with the relative order of their oxidation potential [20]. The HOMO–LUMO energy gap increases in this order.

The molecular orbitals involved in the analysed transitions were examined in detail. The structures of the representative orbitals are displayed in Fig. 3. The compositions of orbitals are quite different for the displacement of ligand L. For N3^{4-}, the HOMO orbital and the subsequent five occupied orbitals are mainly the combinations of the d orbital of ruthenium and p atomic orbital of sulfur and nitrogen in isothiocyanate. In HOMO-3 orbital, the electron density is nearly all located on isothiocyanate. The other five orbitals can be divided into two types according to the bonding property between ruthenium and nitrogen atom in isothiocyanate. There is an antibonding interaction between these two atoms in HOMO-2 to HOMO orbital, while this bonding shows bonding character for HOMO-4 and HOMO-5 orbital. The following six occupied orbitals are mainly located on carboxylate groups. LUMO to LUMO + 7 series of orbitals are π* orbitals of bipyridine in nature with noticeable contribution from carboxylate groups. It will facilitate electron injection as these dyes are anchored on the surface of electrode through carboxylate groups. The LUMO + 8 and LUMO + 9 orbital are another series of Ru-NCS orbitals which

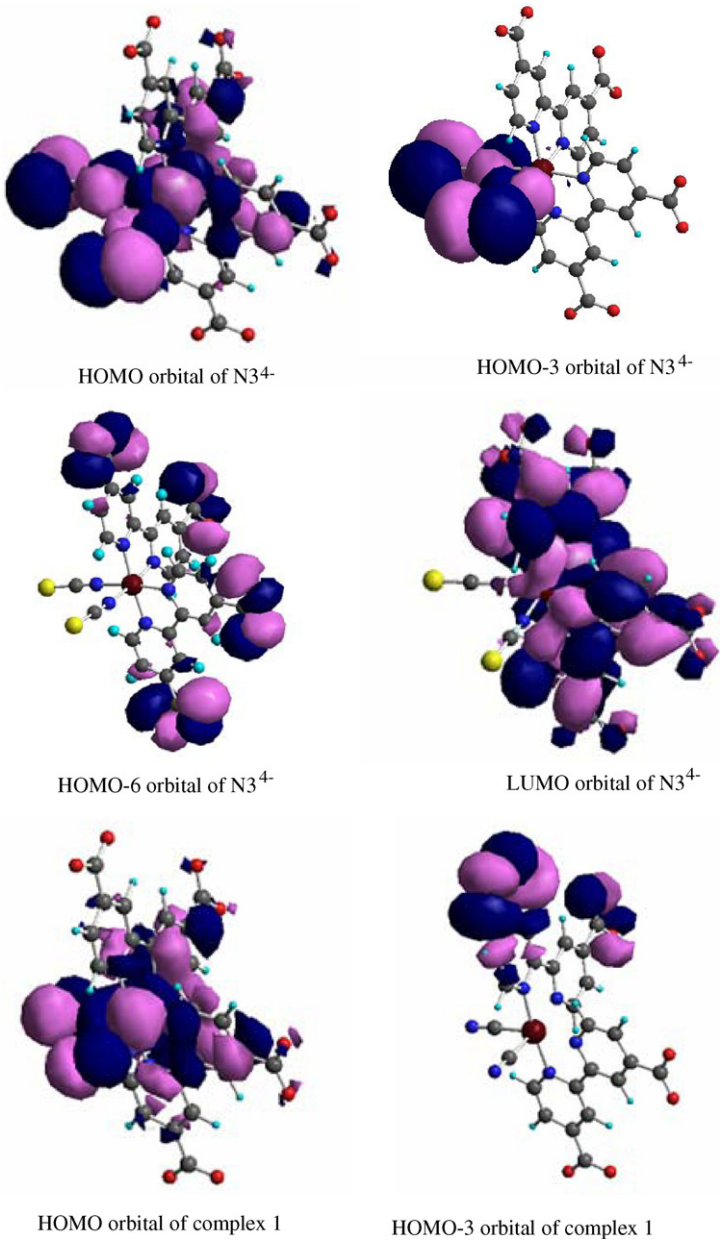

Fig. 3. Structures of the representative orbitals. As the frontier orbitals of complexes **1** and **2**. Share similar characters, only the molecular orbitals of complex **1** are contained in this figure.

display nonbonding property between the metal atom and isothiocyanate.

The frontier orbitals of complexes **1** and **2** seem to share more common characters. As for complexes **1** and **2**, the frontier orbitals can be divided into four types. Their HOMO to HOMO-2 orbital are Ru–ligand L based MOs showing antibonding interaction between Ru and ligand L. This series of MOs is immediately followed by a band of occupied MO located on carboxylate groups. Their distributions of virtual MOs are similar to that of $N3^{4-}$. Most of the involved unoccupied orbitals are based on π* orbitals of bipyridine. The unoccupied orbitals with higher energy level are mainly composed of orbitals of Ru atom.

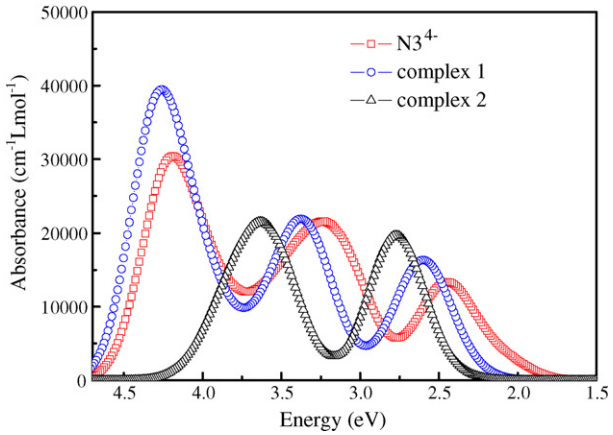

Fig. 4. Comparison of simulated absorption spectra of the three complexes.

The absorption spectra of these three complexes in ethanol were simulated. The calculated spectra were displayed in Fig. 4. Within the scope of wavelength analyzed, the simulated UV–visible absorption spectra of $N3^{4-}$ and complex **1** show three maxima, while the simulated absorption spectrum of complex **2** is composed of two bands. As a whole, the absorption bands of $N3^{4-}$ red-shift compared with the other two complexes. Moreover, $N3^{4-}$ possesses broader absorption band in longer wavelength region (denoted as band I and band II), which is advantage for light harvesting.

The absorption peaks of our simulated spectra as well as the experimental results are summarized in Table 2. The absorption peaks in the visible region band I center at 2.406, 2.604 and 2.765 eV, respectively for $N3^{4-}$, complexes **1** and **2**. Their deviation from the experimental results is less than 0.1 eV. Our results also well reproduce the absorption peaks of band II and III except for band III of $N3^{4-}$ and complex **1**. Their locations blue-shift by 0.229 and 0.266 eV, respectively compared with experimental datum. The similar phenomenon was also discovered in previous research [12]. As a whole, our computational method tends to be effective when dealing with UV–visible absorption spectra of these metal-based dyes with solvation effect.

The characters of transitions were also investigated thoroughly. Part of calculated properties about the singlet excited states of the three complexes are summarized in Table 3. As is shown in Table 3, band I and III of $N3^{4-}$ can be assigned as Ru-isothiocyanate to bipyridine charge transfer (MLCT) and ligand-based charge transfer (LBCT) transition respectively, while band II has mixed character. Most of the excited states in band II are

Table 2
Comparison of the absorption peak energies between the calculated and experimental data of complexes (in eV)

	Band I	Band II	Band III
N3	2.406	3.199	4.191
N3^{exp} [7]	2.322	3.131	3.962
Complex **1**	2.604	3.373	4.266
Complex **1**^{exp} [7]	2.515	3.397	4.000
Complex **2**	2.765	3.636	
Complex **2**^{exp} [20]	2.672		

The experimental data were cited from the references [7] and [20].

Table 3
Part of the calculated properties about the singlet excited states of the three complexes

State	Vertical excitation energies E (eV)	Oscillator strength f	Character[a]
$N3^{4-}$			
Band I			
1	2.0921	0.0300	153 → 154 (94%, MLCT)
5	2.4377	0.1644	151 → 154 (65%, MLCT)
6	2.5841	0.0361	151 → 155 (59%, MLCT)
Band II			
8	3.0526	0.0658	153 → 158 (84%, MLCT)
9	3.0731	0.0429	153 → 157 (75%, MLCT)
12	3.2037	0.0435	152 → 157 (84%, MLCT)
18	3.3232	0.0641	151 → 158 (94%, MLCT)
24	3.4588	0.0376	149 → 154 (47%, MLCT) 145 → 154 (25%, LBCT)
31	3.6718	0.0148	141 → 154 (25%, LBCT)
36	3.7585	0.0019	152 → 163 (49%, d → d*)
Band III			
42	3.9251	0.0296	138 → 154 (71%, LBCT)
43	3.9368	0.0745	137 → 154 (68%, LBCT)
Complex **1**			
Band I			
1	2.3213	0.0083	147 → 148 (97%, MLCT)
5	2.5923	0.2215	145 → 148 (68%, MLCT)
Band II			
11	3.3316	0.1225	146 → 151 (80%, MLCT)
17	3.4796	0.0096	143 → 148 (43%, LBCT)
Band III			
32	3.9871	0.0725	135 → 148 (40%, LBCT)
50	4.2890	0.5094	131 → 148 (59%, LBCT)
Complex **2**			
Band I			
1	2.4567	0.0055	196 → 197 (98%, MLCT)
8	2.7891	0.1313	194 → 199 (26%, MLCT) 195 → 198 (25%, MLCT)
Band II			
17	3.4796	0.0377	196 → 202 (89%, MLCT)
53	3.8273	0.0389	179 → 197 (59%, LBCT)

[a] Only the most relevant transitions are shown in this table.

combined Ru-isothiocyanate to bipyridine transitions in nature; however, excited state 20 to 26 and 37 have mixed MLCT and LBCT character. Excited state 31 to 34, 38 and 39 are essentially LBCT. It is noticeable that state 35 and 36 unambiguously have d → d* transition character. As for complex **1**, its transitions have similar properties as that of $N3^{4-}$ except that there is no unmixed transition with d → d* transition character, while the UV–visible absorption spectrum of complex **2** only shows two peaks. Band I of complex **2** is MLCT in nature, and the other band shows mixed character of MLCT and LBCT.

The light absorption property is the key factor to determine the solar light harvesting efficiency of dyes when they are absorbed onto the surface of the electrode. Dyes with absorption bands in longer-wavelength region are liable to make better use of sunlight. According to our simulated results, the absorption peaks of $N3^{4-}$ in visible region are red-shifted dramatically compared with that of complexes **1** and **2**, which is advantageous for solar light harvesting. Obviously it is one of the predominant causes for the lower efficiency of complexes **1** and **2**.

3.3. The driving force for electron injection

Electron transfer on the dye-semiconductor surface is another crucial factor to determine the overall efficiency of the solar cell. As for polypyridyl ruthenium dyes, a two-state injection model was predicted [21–23]. The ultrafast (<100 fs) component can be attributed to electron injection from nonthermalized excited state, and slow component roots in injection from thermalized excited state.

The electron injection process involves electron transfer from discrete excited states of dyes to a continuum of electronic levels in the semiconductor, so the total electron transfer rate can be

demonstrated as [21,22]:

$$k_{et} = \frac{2\pi}{\hbar}\int_0^{\infty} dE\,\rho(E)|\bar{H}(E)|^2 \frac{1}{\sqrt{4\pi\lambda k_B T}} \times \exp\left(-\frac{(\Delta G^0 + \lambda - E)^2}{4\lambda k_B T}\right) \quad (1)$$

In this equation, $\bar{H}(E)$ is the average electronic coupling between the excited states of dyes and the accepting states in the semiconductor. As has been analyzed in the previous part, LUMO orbitals of these three complexes are all mainly π^* orbitals of bipyridine. The replacement of ligand has little effect on the electronic coupling between the donor and acceptor. $\rho(E)$ denotes the density of accepting states at energy E relative to the conduction band edge. ΔG^0 is the energy gap between the redox potential of excited state dyes and the conduction bend edge of semiconductor $E_{cb} - E_{dye}$. It has been suggested that the relative energetics between the absorbates and conduction band edge of TiO_2 is the most important factor for electron injection [23]. As can be seen from this equation, k_{et} value increases with the more negative value of ΔG^0. In the meantime, the density of accepting state also increases as the E_{dye} value is more negative than the E_{cb} value, so the $E_{cb} - E_{dye}$ value can be denoted as the driving force of the electron injection. According to the two-state injection model, the rate of ultrafast component is in direct proportion to the energy gap between the singlet excited-state redox potential of dyes and the conduction band edge of semiconductor. The rate of the slower component is related to the energy gap between the triplet or the lowest singlet excited-state redox potential of dyes and the conduction band edge of semiconductor because the slower electron injection is supposed to takes place after the intersystem crossing or internal conversion [21–23]. As a whole, larger driving force plays positive effect on the process of electron transfer.

The energy levels of the lowest two excited states absorption peaks for the three dyes and the conduction band edge of TiO_2 are summarized in Fig. 5. As is shown in this figure, the relative order of ^{1}MLCT energy levels is $N3^{4-}$ < complex **1** < complex **2**. The energy gaps to conduction band edge of electrode are 1.03, 0.82 and 0.66 eV for the first singlet band of the three complexes.

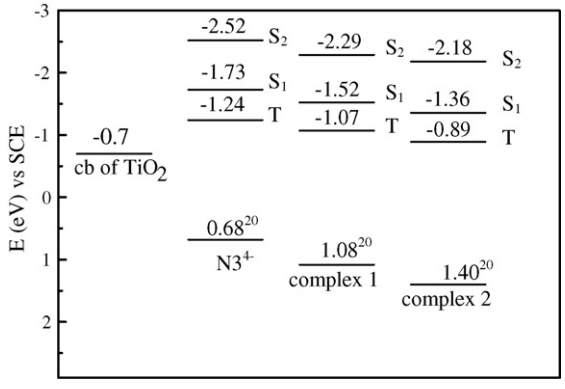

Fig. 5. Energy levels of conduction band of TiO_2, ground and excited state of the three complexes. S_1 and S_2 denote the first and second singlet excited state band peak, while T denotes the first triplet excited state.

For the second band, the energy gaps are 1.82, 1.59 and 1.48 eV respectively. The driving forces for electron injection from non-thermalized singlet excited dye molecules are much larger for $N3^{4-}$ than complexes **1** and **2**.

The transition energetics of triplet state are estimated according to the same geometry in the singlet excited state computation assuming that the time scale of intersystem crossing is short than that of nonradiative relaxation. The energy levels of the first triplet excited states are also summarized in Fig. 5. It is shown that energy gaps versus conduction band edge of the electrode for triplet states are 0.54, 0.37 and 0.19 eV for $N3^{4-}$, complexes **1** and **2**. The driving force for electron injection from the first triplet state decreases in this order after intersystem crossing. The S_1 state of $N3^{4-}$, as the target state of internal conversion, also possesses larger energy gap than the other two complexes.

In summary, both the nonthermalized and thermalized excited states of $N3^{4-}$ possess larger energy gaps than those of complexes **1** and **2**. According to Eq. (1), electron transfer rate to the conduction band of TiO_2 is comparatively higher for $N3^{4-}$. To sum up, $N3^{4-}$ has intense and broad absorption bands as well as favorable energy levels for its excited states. All these characters play positive effect on the its solar to energy efficiency.

4. Conclusion

The light harvesting efficiency and quantum yield of charge injection from the oxidized dye to the conduction band of semiconductor electrode are crucial factors to determine the photoelectrical properties of dyes. These steps of $N3^{4-}$ and its two similar complexes were thoroughly examined with DFT method in our article. Our computational results indicated that variety of ligand L has little effect on the molecular structures of these series of complexes. The electronic structures of dyes vary greatly by the replacement of ligand L. The orbital analysis shows that the orbital compositions of complexes **1** and **2** share more common characters than $N3^{4-}$.

The absorption spectra of the polypyridyl complexes can be well reproduced with theoretical methods in this article. Absorption band I and III of $N3^{4-}$ and complex **1** can be assigned as MLCT and LBCT in nature, while band II has mixed character. According to our computational results, low light harvesting efficiency is probably the main cause for the low efficiency of complexes **1** and **2**.

Energy gaps between the conduction band edge of TiO_2 and excited-state redox potential of dyes can be employed as the driving force for electron injection. The driving forces of ultrafast and slower component for complexes **1** and **2** are much smaller than $N3^{4-}$. The comparatively slower electron injection rate brings out the lower efficiency of complexes **1** and **2**.

In summary, $N3^{4-}$ has not only intense and broad absorption bands but larger driving force for electron injection. These factors are all advantage for its excellent photoelectrochemical performance. Thorough theoretical investigation of these polypyridyl complexes provides us with valuable clue to design new efficient photosensitizer conveniently.

Acknowledgements

Financial support from the program of New Century Excellent Talents in University of China (2005) is acknowledged. All the calculations have been performed at the Fudan High-end Computing Center.

References

[1] B. O' Regan, M. Grätzel, Nature 353 (1991) 737–740.
[2] M. Grätzel, Nature 414 (2001) 338–344.
[3] K. Hara, M. Kurashige, S. Ito, A. Shinpo, S. Suga, K. Sayama, H. Arakawa, Chem. Commun. (2003) 252–253.
[4] T. Horiuchi, H. Miura, K. Sumioka, S. Uchida, J. Am. Chem. Soc. 126 (2004) 12218–12219.
[5] G. Sauvé, M.E. Cass, G. Coia, S.J. Doig, I. Lauermann, K.E. Pomykal, N.S. Lewis, J. Phys. Chem. B 104 (2000) 6821–6836.
[6] M.K. Nazeeruddin, P. Péchy, T. Renouard, S.M. Zakeeruddin, R. Humphry-Baker, P. Comte, P. Liska, L. Cevey, E. Costa, V. Shklover, L. Spiccia, G.B. Deacon, C.A. Bignozzi, M. Grätzel, J. Am. Chem. Soc. 123 (2001) 1613–1624.
[7] M.K. Nazeeruddin, A. Kay, I. Rodicio, R. Humphry-Baker, E. Müller, P. Liska, N. Vlachopoulos, M. Grätzel, J. Am. Chem. Soc. 115 (1993) 6382–6390.
[8] M. Grätzel, J. Photochem. Photobiol. A: Chem. 164 (2004) 3–14.
[9] H. Rensmo, S. Lunell, H. Siegbahn, J. Photochem. Photobiol. A: Chem. 114 (1998) 117–124.
[10] F. Aiga, T. Tada, Sol. Energy Mater. Sol. Cells 85 (2005) 437–446.
[11] J.E. Monat, J.H. Rodriguez, J.K. Mccusker, J. Phys. Chem. A 106 (2002) 7399–7406.
[12] F. De Angelis, S. Fantacci, A. Selloni, Chem. Phys. Lett. 389 (2004) 204–208.
[13] S. Fantacci, F. De Angelis, A. Selloni, J. Am. Chem. Soc. 125 (2003) 4381–4387.
[14] M.K. Nazeeruddin, F. De Angelis, S. Fantacci, A. Selloni, G. Viscardi, P. Liska, S. Ito, B. Takeru, M. Grätzel, J. Am. Chem. Soc. 127 (2005) 16835–16847.
[15] F. De Angelis, S. Fantacci, A. Selloni, M.K. Nazeeruddin, Chem. Phys. Lett. 415 (2005) 115–120.
[16] V. Barone, M. Cossi, J. Phys. Chem. A 102 (1998) 1995–2001.
[17] M. Cossi, V. Barone, R. Cammi, J. Tomasi, Chem. Phys. Lett. 255 (1996) 327–335.
[18] M.J. Frisch, et al., Gaussian 03, Revision C.02, Gaussian Inc., Pittsburgh, PA, 2003.
[19] V. Shklover, Yu.E. Ovchinnikov, L.S. Braginsky, S.M. Zakeeruddin, M. Grätzel, Chem. Mater. 10 (1998) 2533–2541.
[20] G. Sauvé, M.E. Cass, G. Coia, S.J. Doig, I. Lauermann, K.E. Pomykal, N. Lewis, J. Phys. Chem. B 104 (2000) 6821–6836.
[21] J.B. Asbury, E. Hao, Y. Wang, H.N. Ghosh, T. Lian, J. Phys. Chem. B 105 (2001) 4545–4557.
[22] N.A. Anderson, T. Lian, Coord. Chem. Rev. 248 (2004) 1231–1246.
[23] J.B. Asbury, N.A. Anderson, E. Hao, X. Ai, T. Lian, J. Phys. Chem. B 107 (2003) 7376–7386.